A study of the micromechanical push-out test: Response of an SCS-6/Ti-6242 composite

Bérénice Guichet, Jean-Christophe Sangleboeuf, Alain Vassel, Thierry Bretheau

A STUDY OF THE MICROMECHANICAL PUSH-OUT TEST: RESPONSE OF AN SCS-6/Ti-6242 COMPOSITE

Bérénice Guichet,[a,b]* Jean-Christophe Sanglebœuf,[c] Alain Vassel[a] & Thierry Bretheau[c]

[a]*Office National d'Etude et de Recherches Aérospatiales (ONERA), BP 72-92322, Châtillon Cédex, France*
[b]*Laboratoire Matériaux Mécanique Physique, Ecole Centrale de Lyon, 36, ave Guy de Collongue, BP 163, 69131, Ecully, France*
[c]*Laboratoire de Mécanique des Solides, Ecole Polytechnique, 91128 Palaiseau Cédex, France*

Abstract

Push-out tests have been performed on unidirectional SiC-fibre/Ti-6242-matrix composites, with samples of variable thickness and fibre volume fraction. Experimental results show the existence of two distinct decohesion types. SEM observations establish that these two types are characterised by two decohesion sites. Since these mechanisms appear to be linked with geometrical parameters, a finite-element analysis has been developed. This allows us to evaluate the stress field induced by the material manufacture process, the preparation of the sample and the test itself. Two mechanisms are proposed to explain both types of behaviour.

1 INTRODUCTION

The push-out test, like micro-indentation and pull-out test, has been developed over a number of years as a mean of extracting and quantifying the characteristic parameters of the interface between the matrix and the reinforcing fibres. A modelling study, using these parameters, will help the composite designer in optimizing the interface properties of the composite, once included in a structure. The aim of this study is to discover whether the push-out test can give access to the relevant parameters of interface behaviour for inclusion in a dimensional analysis. Push-out tests were performed on titanium–matrix composites reinforced with long SiC fibres, and finite-element modelling, approximating as closely as possible the experimental conditions. The objective is to understand which mechanisms are involved during the test, and which parameters could be deduced. The next step will be to make sure that they are relevant.

*To whom correspondence should be addressed. Fax: 00 33 1 46 73 41 42; e-mail: guichet@onera.fr

2 EXPERIMENTAL PROCEDURE

2.1 Materials

The material of this study is a unidirectional composite with a titanium-alloy matrix; Ti–6Al–2Sn–4Zr–2Mo, reinforced with SCS-6 SiC-fibres. Materials were manufactured by two processes. In the first, the classical foil–fibre–foil process, alternate layers of fibres and titanium foils were pressed at high temperature. The resulting 8-ply composite had an average fibre volume fraction of 0·45, but the fibre distribution was not well controlled. The second process required two steps. Each fibre was coated with the Ti-alloy matrix by physical vapour deposition (PVD), and the coated fibres were then consolidated in a titanium sheath by hot isostatic pressing (HIP). This technique allows us to control the fibre volume fraction of the final composite, which depends on the thickness of the titanium deposit. In this case, the fibre distribution was close to a regular hexagonal array. Except on the external layers, the fibres were never in contact, as can occur in the foil–fibre–foil material. Three composites of volume fraction 0·3, 0·5 and 0·7 were fabricated. Measurement of V_f by image analysis revealed that V_f varied along the composite rod because the titanium deposit is thicker in the middle than at the edge of the fibres. In addition, image analysis permits the measurement of local variation in $V_{???}$; for the PVD + HIP composites the variations are, respectively, 7, 9 and 10%, whereas for the foil–fibre–foil composite the variation is 20%.

The SCS-6 fibre has a 3 μm turbostratic carbon coating, enriched with SiC particles. The graphite planes are mostly oriented perpendicular to the radial direction.[1] Composite consolidation leads to a strong reaction between this carbon coating and the Ti-6242 matrix. An X-ray observation of the interfacial zone reveals that a part of this coating is transformed into reaction products: a 0·5 μm layer of TiC close to the carbon coating and a very thin layer of silicide $(Ti,Zr)_xSi_y$ close to the matrix.[2]

2.2 The push-out device

The push-out apparatus has been developed in order to provide axisymmetrical loading to the fibre, and to be as stiff as possible (Fig. 1). The stiffness is estimated to be $2600\,\mathrm{kN\,m^{-1}}$. The fibre is loaded with a flat WC cylindrical indentor of $100\,\mu\mathrm{m}$ diameter. The hole aligned with the fibre is $200\,\mu\mathrm{m}$ in diameter. The bearer pushes the fibre on the indentor at a speed of $45\,\mu\mathrm{m\,m^{-1}}$. An inductance sensor measures the relative displacement, u, of the indentor relative to the surface sample with a precision of $3\,\mu\mathrm{m}$. The load, F, is recorded by a load cell as a function of the displacement, u, with a precision of 0·1 N. Every fibre is pushed back into the slice before the following test.

3 EXPERIMENTAL RESULTS

3.1 Tests

The test samples are slices cut tranverse to the 0° direction, both faces being mechanically polished after cutting. The titanium sheath from the PVD + HIP process still remains around the composite. The thicknesses of the slices is limited by the WC indentor strength. For the foil–fibre–foil composite, the thicknesses tested were about 160 and $350\,\mu\mathrm{m}$. For the PVD + HIP material, the thicknesses were about 160 and $300\,\mu\mathrm{m}$.

3.2 Two types of behaviour

Two types of response have been recorded. In type I behaviour (Fig. 2), the load rises linearly until a change of slope (point A) or a small peak occurs. The load then keeps increasing until a maximum value, after which it decreases. In type II behaviour, the load increases linearly to a maximum value (point B) that may be twice as high as the load reached at point A in type I behaviour. The load then suddenly drops and eventually reduces more slowly. During the push-back of the fibre, the responses are different. In type I (Fig. 2), the load increases linearly to a peak (point C) at a value lower than the value reached at the end of push-out. The load then increases slowly as the fibre slides back into the matrix. For type II, the load increases up to the value reached at the end of push-out, and then the fibre slides

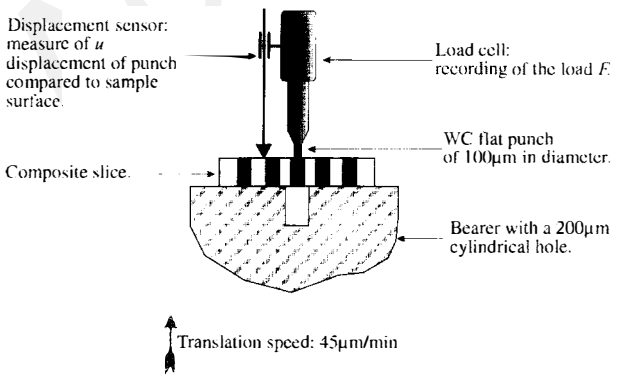

Fig. 1. Schematic illustration of push-out apparatus.

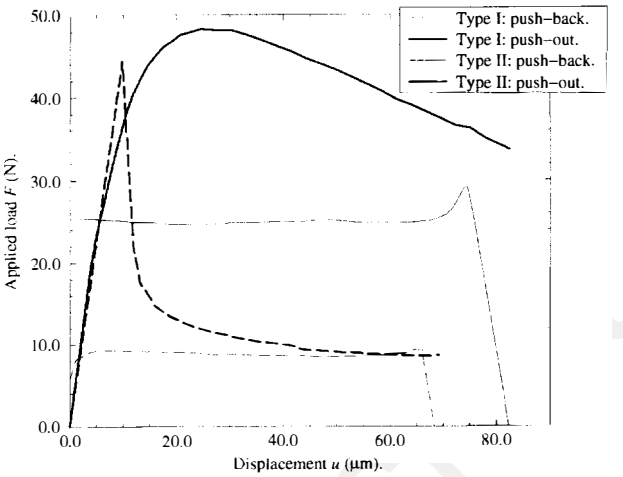

Fig. 2. Load/displacement curves: type I and type II responses.

at almost constant load. When the fibre reaches its initial position, the load drops slightly.

3.3 Microscopical observations

To understand the phenomena linked with both types of behaviour, each side of the sample is examined by scanning electron microscopy at different stages in the test.

Type I: during the linear increase in load, decohesion sometimes occurs on the bottom face of the sample. This failure is localised within the inner layers of the carbon coating on the fibre, close to the SiC. After the change of slope (point A in Fig. 2), the failure is visible on both sides of the slice and remains in the inner layers of the carbon coating. The outer layers remain coherent with the reaction products and the matrix. At the maximum load, or after, the fibre appears to be covered with debris (Fig. 3) which are the inner layers of the coating that have been broken up. During push-back, these debris will stay on the sample surface.

Type II: observations do not reveal any failure before the maximum load (point B on Fig. 4). But after the load drop, the fibre may have slid $10\,\mu\mathrm{m}$. Decohesion occurs strictly between the carbon coating and the

Fig. 3. SEM pictures of fibre after a type I response.

Fig. 4. SEM pictures of fibre after a type II response.

reaction zone. The whole coating remains adherent on the fibre during the conclusion of push-out, and also during push-back.

Both decohesion types are consequently characterized by two distinct sites of decohesion. In an initial approach, values reached at the change of slope (point A in the case of type I, and point B in the case of type II) will be regarded as the point of decohesion (F_d). The decohesion load in type I is always lower than the decohesion load in type II.

3.4 Geometrical parameters linked with push-out behaviour.

The results on the PVD + HIP composites are slightly scattered in respect of both the decohesion load and the mechanism involved. The tests allow identification of the parameters linked with decohesion types. For the $V_f = 0{\cdot}3$ material, only type I occurs whatever the fibre and sample thickness. For the $V_f = 0{\cdot}7$ material, only type II occurs except for the peripheral fibres. In the $V_f = 0{\cdot}5$ composite, both types of behaviour are encountered in a thin sample, whereas only type II occurs in thicker samples.

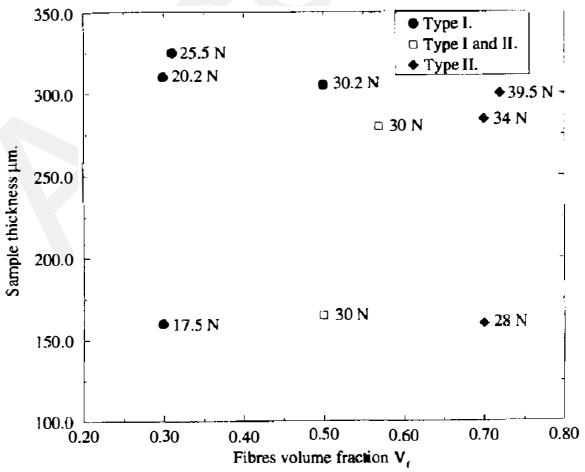

Fig. 5. Debonding types depending on volume fraction and sample thickness with the debonding load.

The behaviour of the foil–fibre–foil composite is more scattered. The response to the test seems to be linked with the local V_f.

The debonding type has been represented for the PVD + HIP material, as a function of the decohesion load in Fig. 5. This shows the influence of sample thickness and fibre volume fraction on the response to push-out testing. It also shows the tendency of the debonding load to increase with fibre content.

4 FINITE-ELEMENT MODELLING OF THE TEST

4.1 Purpose of modelling

The behaviour of only the PVD + HIP materials is studied here since their axisymetric geometry allows very close modelling.

After hot isostatic pressing, cooling of the material induces high residual stresses because of the thermal expansion coefficient mismatch. The interactions of the fibres—depending on their spatial distribution—add perturbations. Moreover, the titanium sheath used in consolidation also contributes to the residual stress fields in the material. Preparation of the composite slices releases part of these residual stresses but it also creates a residual shear stress which does not exist in the bulk material.

Thus, the residual stress field is extremely complex since it results from thermal effects, free-edge effects, fibre distributions (not taken into account in this study), and global fretting. This is why a finite-element analysis is chosen to describe the highly complex stress field in this composite, and its variation during loading.

4.2 The model

The model is defined to replicate the sample geometry and test conditions as closely as possible. It consists of four coaxial cylinders (Fig. 6). The closest neighbourhood of the fibres is not taken into account, despite its influence as shown by Durodola and Derby.[3] These effects require a three-dimensional model as carried out in another study and not presented here.

The SCS-6 fibre is modelled as a 71 μm radius cylinder. Its behaviour is taken to be isotropic and elastic over the temperature range concerned. Data proposed

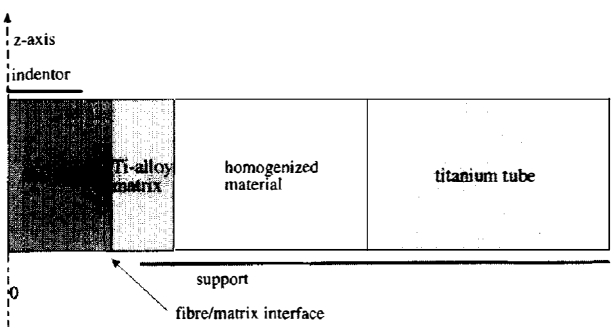

Fig. 6. Finite-element model.

in the literature are quite scattered and the properties suggested by Nimmer *et al.*[4] are chosen. At room temperature, Young's modulus is 407 GPa, Poisson's ratio is 0·2, and the coefficient of thermal expansion is $4{\cdot}65\times10^{-6}\ °C^{-1}$. The coating and the reaction zone are not represented by separated media, mainly because of a lack of data concerning their behaviour.

The matrix is also represented as an isotropic elastic medium, of which the thickness depends on the volume fraction. There are few data on Ti-6242 and again the data determined by Nimmer *et al.*[4] were chosen. At room temperature, Young's modulus is 117 GPa, Poisson's ratio is 0·3 and the coefficient of thermal expansion $12{\cdot}06\times10^{-6}\ °C^{-1}$. There is not yet an interfacial law between the fibre and the matrix: the interface is supposed to be perfect, and decohesion is not modelled.

Fibres and matrix are surrounded by a homogenized material, of which the external radius is 1000 μm, which represents the composite surrounding the tested fibre. As the fibre distribution is periodic and quasi-hexagonal, this medium is taken to be transversely isotropic. Its properties are calculated by using the technique of homogenisation of periodic media with the data used for the fibre and the matrix calculated for each volume fraction (0·3, 0·5 and 0·7) at different temperatures.

The last cylinder represents the titanium sheath from the composite fabrication process. Its external radius is 4500 μm, and its properties are the same as those of the matrix.

The calculations are run for the three volume fractions and for two thicknesses, 160 and 320 μm. Loading is carried out in two steps: first the cooling from 900°C to room temperature, and then the loading of the fibre edge on a 50 μm radius surface, which simulates the indentor pressure. The applied load was 25 N in every case. On the bottom face of the sample, the structure is blocked in the vertical direction from 100 μm of the revolution axis.

The variations of the radial stress, σ_{rr}, and the shear stress, σ_{rz}, along the fibre/matrix interface are studied. Those components are continuous at this interface.

4.3 Results of modelling

The variations of σ_{rr} and σ_{rz} along the interface are plotted for the three volume fraction. After the thermal loading (Figs 7 and 8) σ_{rr} is symmetrical with the centre

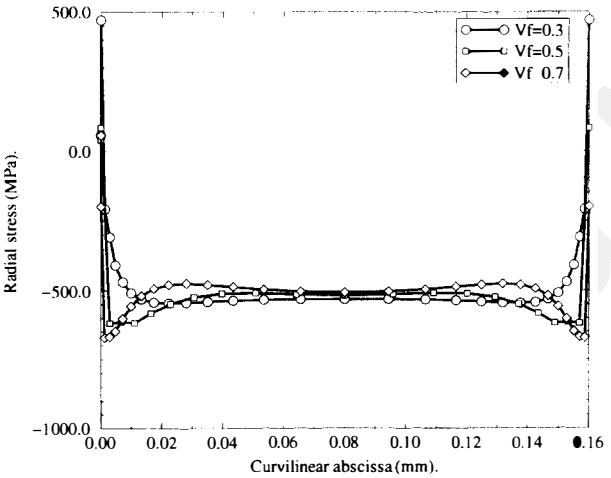

Fig. 7. Thickness = 160 μm, σ_{rr} after the thermal loading.

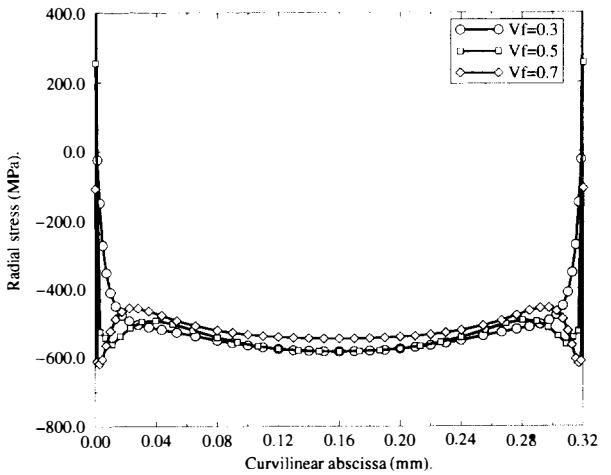

Fig. 8. Thickness = 320 μm, σ_{rr} after the thermal loading.

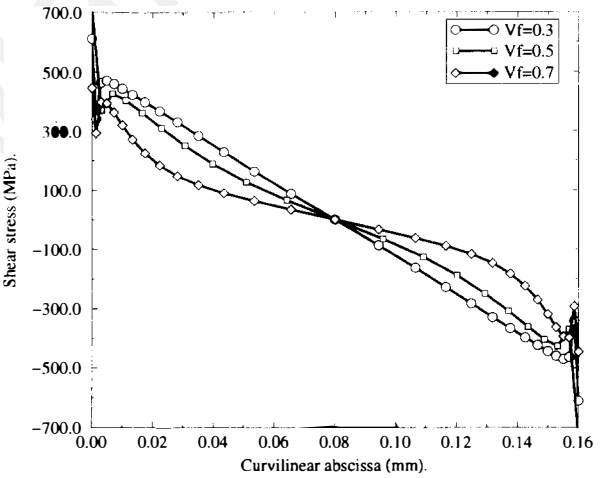

Fig. 9. Thickness = 160 μm, σ_{rz} after the thermal loading.

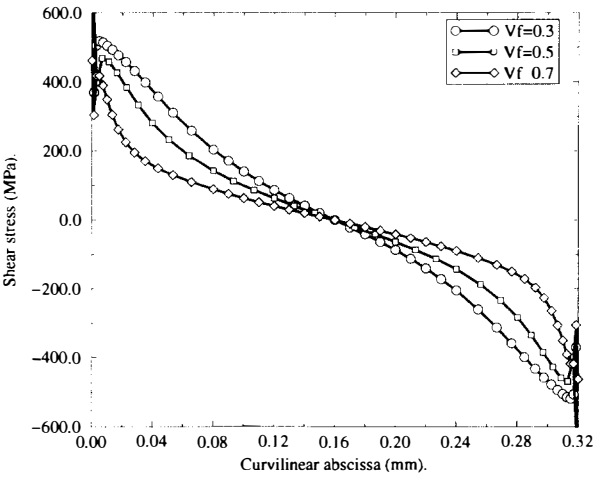

Fig. 10. Thickness = 320 μm, σ_{rz} after the thermal loading.

of the slice, and the interface is mostly under compression. On the other hand, σ_{rz} is antisymmetrical with the centre of the slice (Figs 9 and 10).

For a geometry and a loading very close to the model described here, Kokini and Perkins[5] show that the free surface induces a singularity at the edges of the interface. This is why both radial and shear stresses are divergent at the surfaces of the slice. We note that this divergence is limited to the extreme nodes of the interface.

Nevertheless, free-edge effects depend on the volume fraction. For the higher volume fractions, 0·5 and 0·7, interfacial compression increases close to the free surfaces, whereas for the lower volume fraction, 0·3, interfacial compression decreases. Moreover, the values reached by σ_{rr} are very close at the centre of the slices, whereas it was supposed to diminish at higher V_f. This effect is due to the titanium sheath. It adds a global fretting stress which is higher for the composite of maximum volume fraction; the titanium sheath tends to regroup the level of compression. Without it, the radial compression is -150 MPa for the highest V_f, and -400 MPa for the lowest V_f, in the center of the slice. The titanium sheath has therefore to be taken into account. The variation of σ_{rz} also depends on the volume fraction: it is almost linear for the lowest V_f, whereas it tends to zero faster for the highest V_f (Figs 9 and 10) The free-edge effect is even more marked in the thickest sample, even though it is attenuated in the center of the slice. The residual shear-stress level reached close to the sample surface is still higher for the 160 μm sample than for the 320 μm sample. These results can be compared to those of Chandra and Ananth[6] in a study of metal-matrix composites where the Ti-alloy plasticity is taken into account.

When the top of the fibre is loaded, compression increases close to the indentor because of the Poisson effect. Conversely, compression decreases on the bottom face (Figs 11 and 12). For the $V_f = 0{\cdot}3$ composite the interface is even under tension at about 10 μm from the free surface. The shear stress disminishes close to the indentor but increases on the opposite face (Figs 13 and 14).

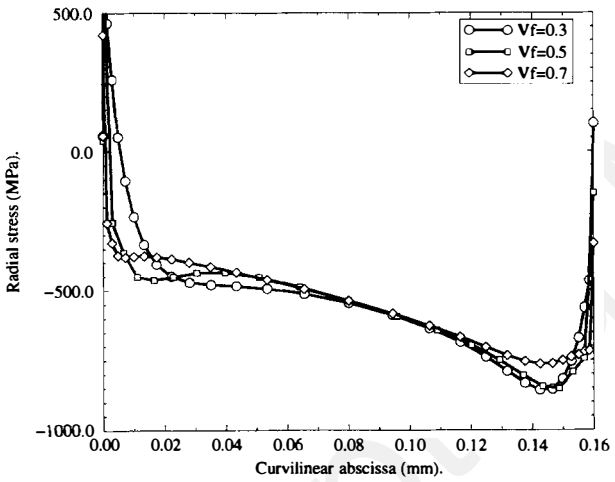

Fig. 11. Thickness = 160 μm, σ_{rr} after the application of the load.

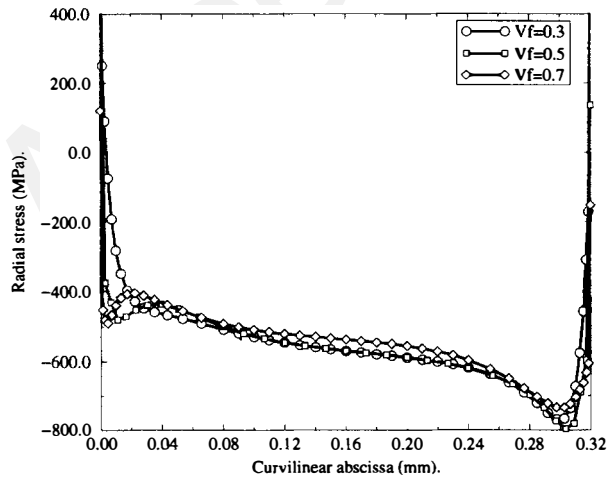

Fig. 12. Thickness = 320 μm, σ_{rr} after the application of the load.

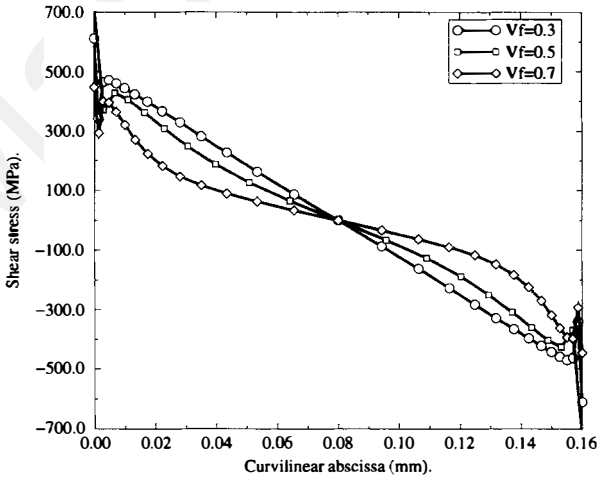

Fig. 13. Thickness = 160 μm, σ_{rz} after the application of the load.

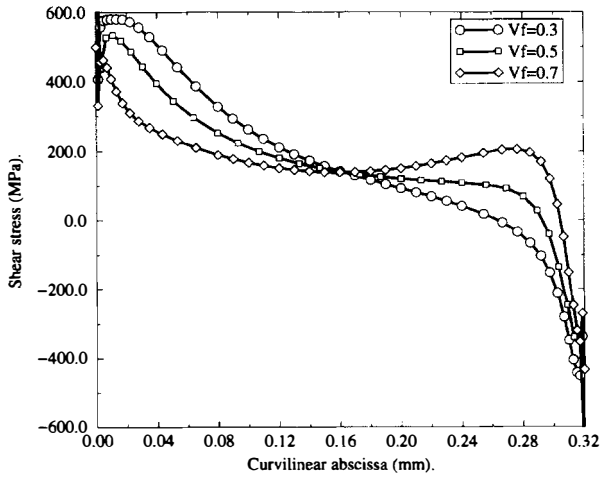

Fig. 14. Thickness = 320 μm, σ_{rz} after the application of the load.

It increases more for the lowest V_f, but the increasing is more uniform for the maximum V_f composite.

5 DISCUSSION AND CONCLUSION

In the case of the lowest volume fraction, the debonding is always by a type-I mechanism. During type-I decohesion, initiation of failure occurs at a low load level within the turbostratic carbon, on the bottom face of the sample, as observed by Ghosn *et al.*.[7] When load is applied, the interface is in tension on the bottom face of the sample. Decohesion may occur in the turbostratic carbon, because the graphite planes are slightly linked in this loading direction. Since the shear stress is also high at this point, the failure can propagate along the interface. Nevertheless σ_{rz} is high only locally, and it decreases rapidly, which is why the failure propagation can be stable. The last point to note is that the failure does not remain in the same propagation plane, so that the carbon coating is broken up, and the fibre appears to be covered with debris (Fig. 3). The sliding surface of the fibre is then very rough, which induces high friction. This is why the load needed to push out the fibre is high.

Eventually, as the coating does not go back into the slice, the load required to push the fibre back is lower than the load required to push it out.

In the case of the highest volume fraction, the decohesion mechanism is always type II (except for the peripheral fibres). During this type of debonding, no failure appears before the maximum load and the fibre slides suddenly. When the fibre is loaded, the interface carries quite a uniform shear stress. When the shear stress reaches a critical value, the interface breaks suddenly. Under this type of loading, the decohesion occurs between the carbon coating and the reaction zone. Moreover, the failure propagates without producing any debris, as can be seen from Fig. 4, so that the sliding surfaces are very smooth, and the fibre is extracted at a lower load than in type I.

The model shows that to reach the same shear stress level in the low and in the high volume fraction cases, the load needed in the former case is higher. This explains the differences in the decohesion load that has been observed (Fig. 5).

Eldridge and Ebihara[8] also found these two types of debonding, but by making tests at various temperatures. They tested a Ti-15 3 alloy reinforced with SCS-6 fibres. The volume fraction of the material was about 0·35. The response of the composite depends on the temperature. At room temperature, the behaviour is similar to a type-I behaviour, whereas at 400°C space it resembles type-II behaviour. We may deduce from our study that when the test is performed at higher temperature, the level of residual stresses is reduced, and the behaviour of the material becomes close to that observed at room temperature for the maximum volume fraction material.

The push-out tests and the finite-element analysis allow us to identify two distinct debonding mechanisms in the same material at the same temperature. We also find that the residual stress field has an important role in determining the interfacial decohesion.

This study shows that the use of the push-out test to obtain interfacial data in order to model the behaviour of the bulk composite is quite hazardous. Particularly, we have to be sure that the decohesion involved in the push-out test is the same as the mechanism occurring in the massive material.

We note that the influence of the neighbouring environment of the fibre has to be taken into account in order to analyse more precisely the stress fields along the interface and their variations during thermal and mechanical loading.

REFERENCES

1. Li, D. S. and Wisnom, M. R., Micromechanical modelling of SCS-6 fibre reinforced Ti-6Al-4V under transverse tension—effect of fibre coating. *J. Compos. Mater.*, 1996, **30**, 1289–1305.
2. Vassel, A., Interface considerations in high-temperature titanium metal matrix composites. *J. Micros.*, 1997, **185**, 303–309.
3. Durodola, J. F. and Derby, B., An analysis of thermal residual stresses in Ti-6 4 alloy reinforced with SiC and Al_2O_3 fibres. *Acta Metall. Mater.*, 1994, **42**, 1525–1534.
4. Nimmer, R. P., Siemers, P. A. and Eggleston, M. R., Fibre array geometry effects upon tranverse tensile behaviour of SiC/Ti composites. *Compos. Eng.*, 1994, **4**, 1289–1588.
5. Kokini, K. and Perkins, R. W., Free edge thermal singularities in finite concentric cylinders. *Computers and Structures*, 1984, **19**, 531–534.
6. Chandra, N. and Ananth, C. R., Analysis of interfacial behaviour in MMCs and IMCs by the use of thin-slice push-out tests. *Compos. Sci. Technol.*, 1995, **54**, 87–100.
7. Ghosn, L. J., Eldridge, J. I. and Kantzos, P., Analytical modeling of the interfacial stress state during push-out testing of SCS-6/Ti-based composites. *Acta Metall. Mater.*, 1994, **42**, 3895–3908.
8. Eldridge, J. I. and Ebihara, B. T., Fibre push-out testing for elevated temperatures. *J. Mater. Res.*, 1994, **9**(4), 1035–1042.